JACS
JOURNAL OF THE AMERICAN CHEMICAL SOCIETY
Article
pubs.acs.org/JACS

Development of a Long-Range Surface-Enhanced Raman Spectroscopy Ruler

Anant Kumar Singh, Sadia Afrin Khan, Zhen Fan, Teresa Demeritte, Dulal Senapati, Rajashekhar Kanchanapally, and Paresh Chandra Ray*

Department of Chemistry, Jackson State University, Jackson, Mississippi 39217-0510, United States

ABSTRACT: Optical-ruler-based distance measurements are essential for tracking biomolecular processes in a wide range of analytical biochemical applications. The normally used Förster resonance energy transfer (FRET) ruler is not useful for investigating distance-dependent properties when distances are more than 10 nm. Driven by this limitation, we have developed a long-range surface-enhanced Raman spectroscopy (SERS) optical ruler using oval-shaped gold nanoparticles and Rh6G dye-modified rigid, variable-length double-strand DNAs. The bifunctional rigid dsDNA molecule serves as the SERS-active ruler. Our experimental results show that one can tune the length of the SERS ruler between 8 and ∼18 nm by choosing the size of the oval-shaped gold nanoparticles. A possible mechanism for our observed distance-dependent SERS phenomenon is discussed using the Gersten and Nitzan model. Ultimately, our long-range SERS molecular rulers can be an important step toward understanding distance-dependent biological processes.

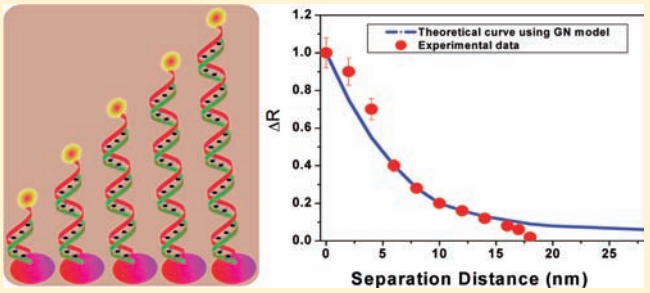

INTRODUCTION

Distance measurements based on an optical spectroscopy ruler are essential for tracking biomolecular conformational changes, drug discovery, and cell biology.[1−3] In 1967, Förster resonance energy transfer (FRET) was used for the first time by Stryer and Haugland as a "spectroscopic ruler" to measure distances in macromolecules.[1] Stryer and Haugland's report opened a new window on the use of optical rulers based on FRET to investigate a wide range of biological activities, which can now be used for obtaining distance information on a single-biomolecule level.[2,3] The FRET process results from dipole−dipole interactions; as a result, the energy-transfer process is strongly dependent on the center-to-center separation.[1−3] It also requires a nonzero integral of the spectral overlap between donor emission and acceptor absorption.[1−3] This fact limits the length scale of FRET rulers to a maximum of 10 nm, as discussed in several articles.[3−5] Due to the distance limitation, normal FRET optical rulers are not suitable for investigation of biological structural change phenomena for large biological systems, where the donor and acceptor distances are much more than 10 nm.[6−8] This fact prompted scientists to look for a long-range optical ruler that could be used for monitoring biological processes above the 10 nm scale.[9−11] Recently, several groups including ours have reported that the limitations of the FRET optical ruler can be overcome with a long-range plasmonic[12−15] and nanoparticle-based surface energy-transfer (NSET) ruler.[16−18]

The possibility of observing very weak normal Raman signals, with enhancements on the order of 10^6−10^{14} in the presence of a metal nanomaterial surface,[19−23] makes surface-enhanced Raman spectroscopy (SERS) very attractive for ultrasensitive biological[24−27] and chemical sensing.[28−31] In addition to sensitivity, another important feature of SERS is the level of detection specificity that usually achieved by controlling the chemistry around the metal surface.[32−35] After incorporating a specific chemical or biological moiety on the surface, one can target the detection of a single species present in a complex sample mixture at the femtomolar level without having to physically separate out interfering species.[36−39] The very high sensitivity along with the highly informative spectral characteristics offered by SERS are very valuable for biological process monitoring.[40−43] As a result, the development of a long-range SERS ruler will be very useful for monitoring biological processes at very low concentration levels. Driven by this need, we report in this article the development of a long-range SERS ruler using oval-shaped gold nanoparticles (AuNPs). We have developed a SERS ruler using an Rh6G dye molecule that is spaced from oval-shaped AuNPs of 30 nm diameter by double-strand DNA (dsDNA) of various lengths (Scheme 1). Recently, Parak et al.[17] and Murphy et al.[44] reported that the interaction between AuNPs and DNA can cause the DNA to bend. Park et al.[17] also showed that the more the DNA molecule bonds to the surface, the lesser is the probability of bending. As a result, in the work described in this article, we used ∼100−120 DNA/nanoparticle surface to minimize the bending of the dsDNA. Using dsDNA, the length of the spacer was increased in 0.32 nm steps with the addition of each DNA base pair. Since dsDNA is known to be rigid up to 50 nm persistence length,[45,46] we can assume that the SERS ruler length can be adjusted easily by

Received: March 7, 2012
Published: May 4, 2012

   dx.doi.org/10.1021/ja301921k | J. Am. Chem. Soc. 2012, 134, 8662−8669

Scheme 1. (A) Synthetic Method for Developing a SERS Ruler and (B) Illustration of a SERS Ruler Consisting of 5′-Rh6G- and 3′-SH-Modified dsDNA of Different Lengths Attached to Oval-Shaped Gold Nanoparticles

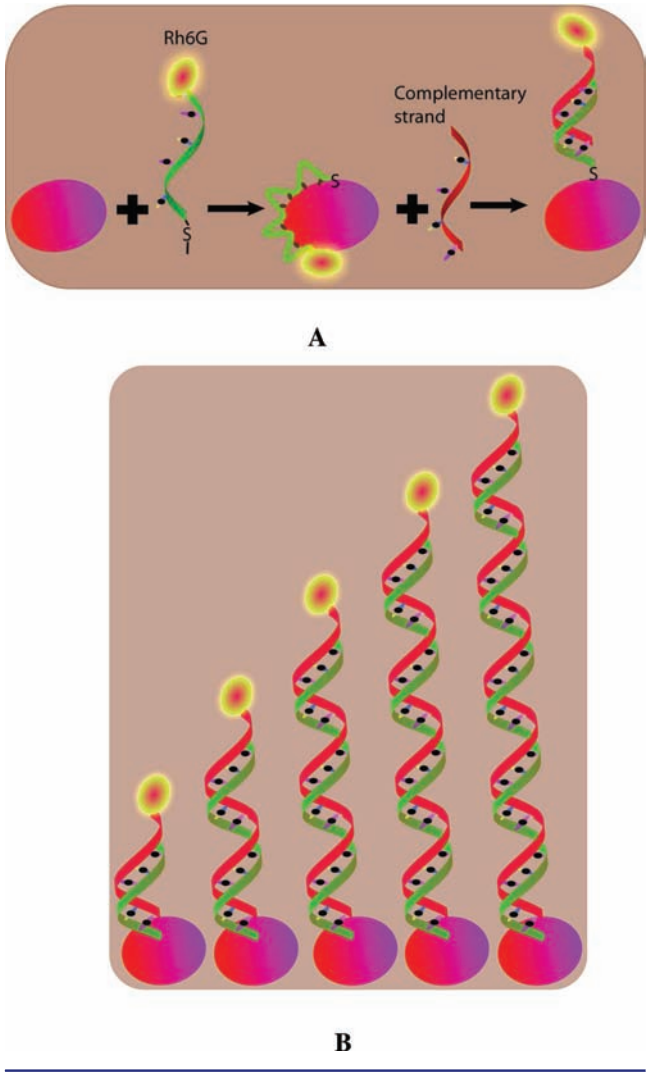

changing the number of base pairs of dsDNA. SERS is often thought of as a near-field phenomenon,[18,20] and it has been reported that SERS occurs when the Raman dye molecules are in close proximity to the nanostructure's surface. SERS enhancement at 120 nm distance has been reported by Mirkin et al.[34] using Au−Ni multisegmented nanowires. In this article, we report that one can tune the SERS ruler length from 8 to ∼20 nm by choosing the size of the oval-shaped AuNPs. To understand our experimentally observed long-range SERS phenomena, we have employed the Gersten and Nitzan (GN) model,[47] where the SERS enhancement factor is described on the basis of the size of the particle and the distance between the nanoparticle surface and Rh6G Raman dye. The GN model[47] is known to be adequate when the nanoparticle size and the Raman molecule−nanoparticle surface distance are small compared to the excitation wavelength,[48−52] which is true in our case.

■ MATERIALS AND EXPERIMENTS

Hydrogen tetrachloroaurate hydrate ($HAuCl_4·3H_2O$), sodium borohydride ($NaBH_4$), cetyl trimethylammonium bromide (CTAB), trisodium citrate, and cystamine dihydrochloride were purchased from Sigma-Aldrich and used without further purification. DNA strands were purchased from Midland Certified Reagent.

Synthesis of Oval-Shaped Gold Nanoparticles. Oval-shaped AuNPs with aspect ratio 1.1−1.2 (Figure 1) were synthesized using a

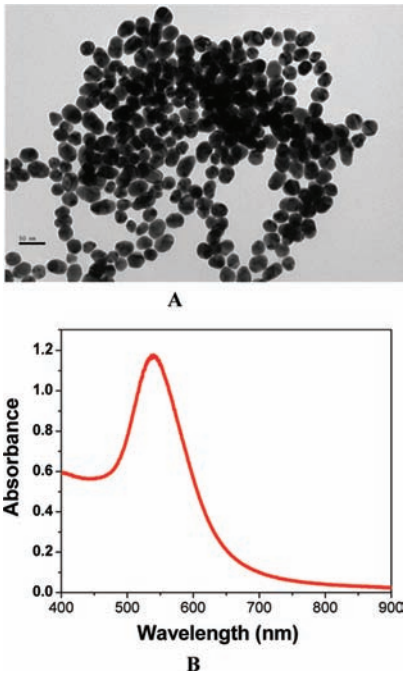

Figure 1. (A) TEM image showing freshly prepared 5′-Rh6G-modified DNA strands conjugated to oval-shaped gold nanoparticles. (B) Absorption profile for 5′-Rh6G-modified DNA strands conjugated to oval-shaped AuNPs. The strong long-wavelength band in the visible region at 550 nm is due to oscillation of the conduction band electrons.

seed-mediated growth procedure in the presence of CTAB, as we reported before.[53] In the first step, very small spherical seed particles are generated using trisodium citrate as a stabilizer and $NaBH_4$ as a strong nucleating agent.[54−57] In the next step, ascorbic acid is used as a weak reductant and CTAB as a shape-templating surfactant so that the seeds can grow into larger particles of the particular morphology we desired.[54−57] The ascorbic anions transfer electrons to the seed particles, which reduces gold ions to form a shell that grows into different shapes in the presence of CTAB.[54−57] Spherical gold seeds were synthesized by mixing aqueous solutions of $HAuCl_4·3H_2O$ w ith trisodium citrate in 20 mL of double-distilled deionized water (18 MΩ) so that the final concentration of $HAuCl_4·3H_2O$ was 2.1×10^{-4} M and the concentration of trisodium citrate was 10^{-4} M. An ice-cooled, freshly prepared aqueous solution of $NaBH_4$ (0.1 M, 55 μL) was then added under vigorous stirring. The solution turned pink immediately after the addition of $NaBH_4$ and became red being kept in the dark overnight. Nanoseeds exhibit absorption spectra with a maximum at 510 nm that corresponds to 4.1 nm seeds, which has been confirmed by transmission electron microscopy (TEM; JEM-2100F). To prepare oval-shaped AuNPs, we used 4.75 mL of 0.0085 M CTAB solution in a small vial, to which we added 0.2 mL of 0.01 M $HAuCl_4·3H_2O$ under constant stirring. After that, we added 0.03 mL of 0.01 M $AgNO_3$ dropwise to allow the solution to mix properly. Once the solution was mixed properly, we added 0.032 mL of 0.1 M ascorbic acid slowly as a reducing agent. The solution turned colorless. To this colorless solution we added gold seeds 0.01 mL at a time and gently mixed the solution for 30 s. The color changed immediately and became dark blue within 2 min. TEM and UV−visible absorption spectroscopy were used to characterize the nanoparticles. The TEM image (Figure 1A) shows that the aspect ratio of the oval-shaped nanoparticles is 1.1−1.2. As shown in Figure 1B, oval-shaped AuNPs

dx.doi.org/10.1021/ja301921k | J. Am. Chem. Soc. 2012, 134, 8662−8669

have only one plasmon band at 550 nm, like spherical AuNPs, but its λ_{max} is shifted by ~35 nm in comparison to that for spherical AuNPs of the same size. The concentration of oval-shaped AuNPs was measured using the plasmon absorption peak at 550 nm, given that the extinction coefficient of the oval-shaped AuNPs is 2.3×10^9 M^{-1} cm^{-1}. The extinction coefficient was measured by using inductively coupled plasma analysis to quantitatively determine the concentration of oval-shaped AuNPs in solution, and the nanoparticle volume was measured by TEM. A similar method was used by El-Sayed et al.[54] and Murphy et al.[55] to measure the extinction coefficients of AuNPs of different shapes. This experiment was performed 4−5 times, and average values are reported in this article.

Synthesis of Single-Strand DNA Attached to Oval-Shaped Gold Nanoparticles. Oval-shaped AuNPs were synthesized using a seed-mediated growth procedure in the presence of CTAB, which is positively charged at physiological pH and, as a result, can easily attract negatively charged proteins. However, CTAB is known to be cytotoxic, so this method will not be ideal for in vivo diagnosis. To overcome this problem, the CTAB surfactant on the surface of oval-shaped AuNPs was replaced by mercaptohexanoic acid using a round-trip phase-transfer ligand-exchange method reported recently by Wijaya et al.[56] After that, 5′-Rh6G- and 3′-SH-modified single-strand DNA (ssDNA) was gradually exposed to oval-shaped AuNPs in the presence of sodium dodecyl sulfate, sodium chloride, and phosphate-buffered saline (PBS) for ~10−12 h. To remove the unbound ssDNA, we centrifuged the solution at 6000 rpm for 20 min, and the precipitate was redispersed in 2 mL of the buffer solution. To measure the number of 5′-Rh6G-modified ssDNA molecules attached on each oval-shaped AuNP after conjugation, we treated the Rh6G-modified DNA-conjugated oval-shaped AuNPs with 10 μM potassium cyanide to oxidize the oval-shaped AuNPs. After that, the solution containing the released Rh6G-labeled DNA was collected for fluorescence spectroscopy analyses. By dividing the total number of Rh6G-labeled DNAs by the total number of oval-shaped AuNPs, we estimated that there were ~100−120 DNAs per oval-shaped AuNP. This experiment was performed 4−5 times, and average values are reported in this article.

SERS Probe for Monitoring Distance-Dependent SERS Activities. For the SERS experiment, we designed a SERS probe, as we reported recently.[39,57] In brief, we used a continuous-wavelength DPSS laser (LUD-670, Laser Glow Technology) operating at 670 nm as an excitation light source. An InPhotonics 670 nm Raman fiber-optic probe was used for excitation and data collection. It combines 90 μm excitation fiber and 200 μm collection fiber with filtering and steering micro-optics. To collect SERS data, we used a miniaturized QE65000 scientific-grade spectrometer from Ocean Optics and Ocean Optics' SpectraSuite spectroscopy data acquisition software.

NSET Study. For the NSET experiment, we used a 532 nm continuous-wavelength OEM laser as an excitation light source. Details of the NSET experimental setup were reported previously by our group.[9−11] In brief, the excitation light source was first attenuated using an appropriate neutral density filter and coupled to the excitation arm of a Y-shaped reflection probe through a plano-convex lens (f = 4.5 mm). We used a miniaturized QE65000 scientific-grade spectrometer from Ocean Optics as a NSET detector, which has remarkable sensitivity for low-light-level applications. All the data were collected using Ocean Optics' SpectraSuite spectroscopy data acquisition software.

Design of Different Length Raman Optical Rulers. To design Raman optical rulers of different lengths, we used 5′-Rh6G- and 3′-SH-modified ssDNA of different lengths. After hybridization with complementary DNA (cDNA), the separation between the oval-shaped AuNPs and Rh6G dye was systematically varied. Capture sequences are shown below:

2mer: 5′-Rh6G-CT-3′-SH
3mer: 5′-Rh6G-CTG-3′-SH
4mer: 5′-Rh6G-CTG G-3′-SH
6mer: 5′-Rh6G-CTG GTC-3′-SH
8mer: 5′-Rh6G-CTG GTC AT-3′-SH
10mer: 5′-Rh6G-CTG GTC ATG G-3′-SH
12mer: 5′-Rh6G-CTG GTC ATG GCG-3′-SH
18mer: 5′-Rh6G-CTG GTC ATG GCG GGC ATT-3′-SH
24mer: 5′-Rh6G-CTG GTC ATG GCG GGC ATT TAA TTC-3′-SH
28mer: 5′-Rh6G-CTG GTC ATG GCG GGC ATT TAA TTC TCG G-3′-SH
30mer: 5′-Rh6G-CTG GTC ATG GCG GGC ATT TAA TTC TCG GGC-3′-SH
34mer: 5′-Rh6G-CTG TTC GCG CTG GTC ATG GCG GGC ATT TAA TTC T-3′-SH
36mer: 5′-Rh6G-CTG TTC GCG CTG GTC ATG GCG GGC ATT TAA TTC TCG-3′-SH
38mer: 5′-Rh6G-CTG TTC GCG CTG GTC ATG GCG GGC ATT TAA TTC TCG GG-3′-SH
42mer: 5′-Rh6G-CTG TTC GCG CTG GTC ATG GCG GGC ATT TAA TTC TCG GGC ACG-3′-SH
45mer: 5′-Rh6G-CTG TTC GCG CTG GTC ATG GCG GGC ATT TAA TTC TCG GGC ACG CCG-3′-SH
52mer: 5′-Rh6G-CTG TTC GCG CTG GTC ATG GCG GGC ATT TAA TTC TCG GGC ACG CCG TAG TTT G-3′-SH
55mer: 5′-Rh6G-CTG TTC GCG CTG GTC ATG GCG GGC ATT TAA TTC TCG GGC ACG CCG TAG TTT GAA G-3′-SH
57mer: 5′-Rh6G-CTG TTC GCG CTG GTC ATG GCG GGC ATT TAA TTC TCG GGC ACG CCG TAG TTT GAA GTT-3′-SH

RESULTS AND DISCUSSIONS

To design the SERS ruler, we first attached 5′-Rh6G- and 3′-SH-modified ssDNA to oval-shaped AuNPs via thiol-gold chemistry (Scheme 1). In this case, due to the conformationally flexible backbone of ssDNA, a favorable conformation for the attached oligomers is an archlike structure in which both the 3′ and 5′ ends are attached to the particle.[9−11] To understand whether Rh6G dyes at the distal end can loop back and adsorb onto the surface of the same oval-shaped AuNPs, as shown in Scheme 1, we performed SERS and NSET experiments. Our experimental data (Figure 2A) showed a quenching efficiency of nearly 99%, which clearly indicates that Rh6G was statically adsorbed on the oval-shaped gold particle surface. Some insight came from SERS studies in Figure 2, which showed that Rh6G dyes are reversibly adsorbed on the surface of colloidal AuNPs; as a result, we observed very strong SERS signal enhancement. The Raman modes at 236, 252, 273, and 376 cm^{-1} in Figure 2B are the N−C−C bending modes of the ethylamine group of the Rh6G ring, and the Raman modes at 615, 778, 1181, 1349 1366,1511, 1570, 1603, and 1650 cm^{-1} are due to C−C−C ring in-plane bending, C−H out-of-plane bending, C−N stretching, and C−C stretching, as we reported before.[57]

The Raman enhancement factor, G, was measured experimentally by direct comparison of normal Raman spectra,[20−34,57]

$$G = \frac{[I_{SERS}]}{[I_{Raman}]}\frac{[M_{bulk}]}{[M_{ads}]} \quad (1)$$

where I_{SERS} is the intensity of the 1511 cm^{-1} vibrational mode of Rh6G in the surface-enhanced spectrum, and I_{Raman} is the intensity of the same mode in the bulk Raman spectrum. M_{bulk} is the number of molecules used in the bulk, and M_{ads} is the number of molecules adsorbed and sampled on the SERS-active substrate. All spectra are normalized for the integration time. The enhancement factor, estimated from the SERS signal and normal Raman signal ratio for the 1511 cm^{-1} band, is ~4.5×10^6.

dx.doi.org/10.1021/ja301921k | J. Am. Chem. Soc. 2012, 134, 8662−8669

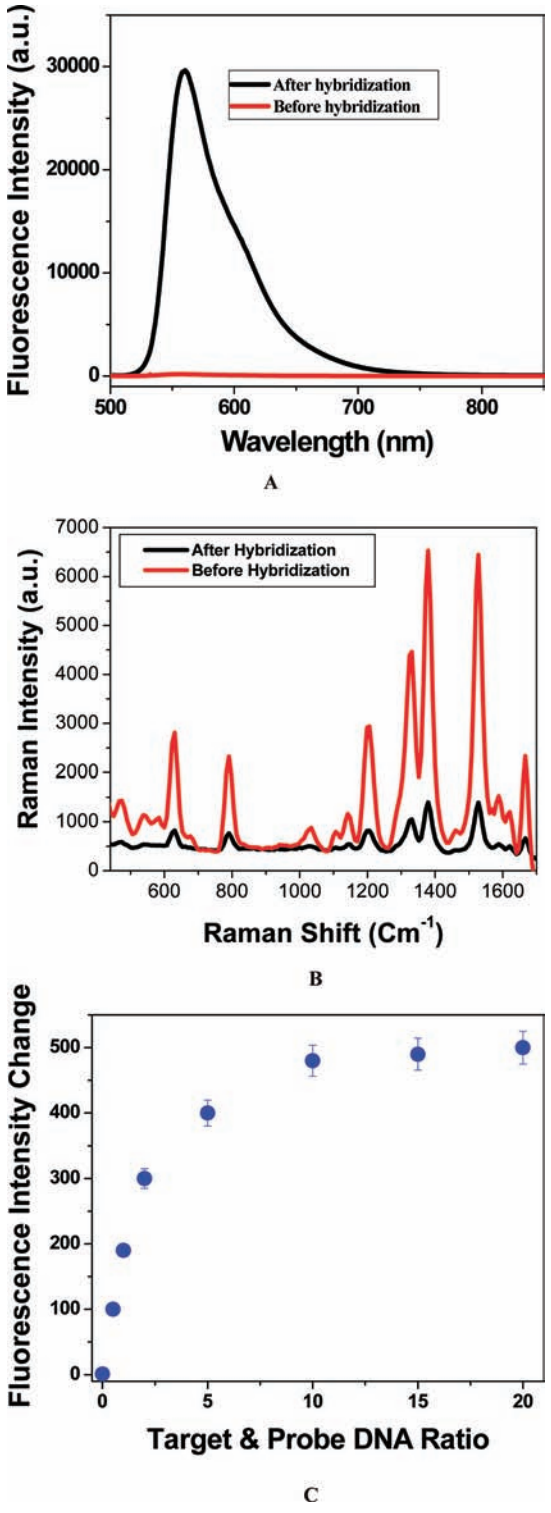

Figure 2. (A) Fluorescence intensity from 5′-Rh6G- and 3′-SH-modified 52mer ssDNA before and after hybridization when DNA strands were attached to oval-shaped gold nanoparticles though −SH linkage. (B) SERS intensity from 5′-Rh6G- and 3′-SH-modified 30mer ssDNA before and after hybridization when DNA strands were attached to oval-shaped AuNPs though −SH linkage. (C) Fluorescence response upon the addition of different concentrations of target DNA to 5′-Rh6G- and 3′-SH-modified 45mer probe DNA attached to oval-shaped AuNPs. In this experiment we varied the concentration ratio of target DNA to probe DNA from 0.5 to 20.

No significant changes in Raman frequencies are observed in comparison to the corresponding SERS and Raman bands.

Hybridization was performed using a 1:10 ratio of probe-to-target sequences in 10 mM PBS solution containing 0.3 M NaCl. To remove the unbound ssDNA target, we centrifuged the solution at 6000 rpm for 20 min and then redispersed the precipitate in 2 mL of the buffer solution. Upon hybridization with cDNA, due to the duplex structure, the dsDNA does not adsorb onto the oval-shaped AuNPs surface, as shown in Scheme 1A. As a result, after hybridization, fluorescence persists and the SERS intensity decreases (Figure 2A,B). To quantify the extent of DNA hybridization, fluorescence was measured as a function of target strand concentration. In Figure 2C, the fluorescence intensity increases until the target and probe DNA ratio is 1:10, and then it remains almost the same. To make sure that the hybridization was almost complete, we used a 1:10 ratio of probe-to-target sequence. Now, after hybridization, the separation distance between the nanoparticle and the Rh6G dye can be evaluated using the simple model reported by Clegg et al.[45] The distances are estimated by taking into account the size of the Rh6G dye, 0.32 nm for each base pair, and 1.8 nm for Au−S distance + base pair-to-dye distance. Duplex DNA lengths of less than 100 base pairs are typically assumed to be adequately modeled by a rigid-rod approximation with only high-frequency oscillations along the backbone, as described by Hagerman.[46] Our experimental results (Figure 2B) clearly show that, though after hybridization the distance between oval-shaped AuNPs and Rh6G Raman dye is more than 10 nm, a significant SERS signal can be observed, which is remarkable. To understand whether our assumption of the rigid-rod approximation is valid, we used dynamic light scattering (DLS) measurement as well as the NSET experiment. DLS measurement was performed using a Malvern Zetasizer Nano instrument. Our DLS data indicate that our synthesized oval-shaped AuNPs have an average size of ∼30 ± 2 nm, which can be seen clearly from our TEM data. In the case of 5′-Rh6G- and 3′-SH-modified 30mer ssDNA attached to AuNPs, after hybridization the diameter changes to ∼53 ± 2 nm. Our DLS experiment indicates that the distance between AuNPs and Rh6G dye is ∼11.5 nm, which is very close to our estimated distance of 11.4 nm. In the same way, we also measured the end-to-end distance between AuNPs and Rh6G dye for other DNAs of different lengths, and our results indicate that the DLS measurement data are quite close to our estimated distances.

As we have discussed before, several groups including ours[5−11] have experimentally demonstrated that the NSET ruler is capable of measuring distances more than twice the FRET distance. As a result, we also performed NSET experiments to measure the distance between Rh6G and the oval-shaped AuNPs surface. After hybridization, by varying the cDNA lengths, the separation between oval-shaped AuNPs and Rh6G dye was systematically varied between 3 and 20 nm by varying the number of base pairs.

Figure 3A shows how the quenching efficiency varies with increasing distance between 30 nm oval-shaped AuNPs and Rh6G dye. The quenching efficiency for each sample was measured by comparison against control dsDNA−Rh6G dye in the absence of NPs, using the following equation:[4−11]

$$Q_{\mathrm{eff}} = 1 - \frac{I_{\mathrm{sample}} A_{\mathrm{control}}}{I_{\mathrm{control}} A_{\mathrm{sample}}} \qquad (2)$$

where Q_{eff} is the quenching efficiency due to NSET, I_{sample} and I_{control} are the integrated intensities under the curve for the

dx.doi.org/10.1021/ja301921k | J. Am. Chem. Soc. 2012, 134, 8662−8669

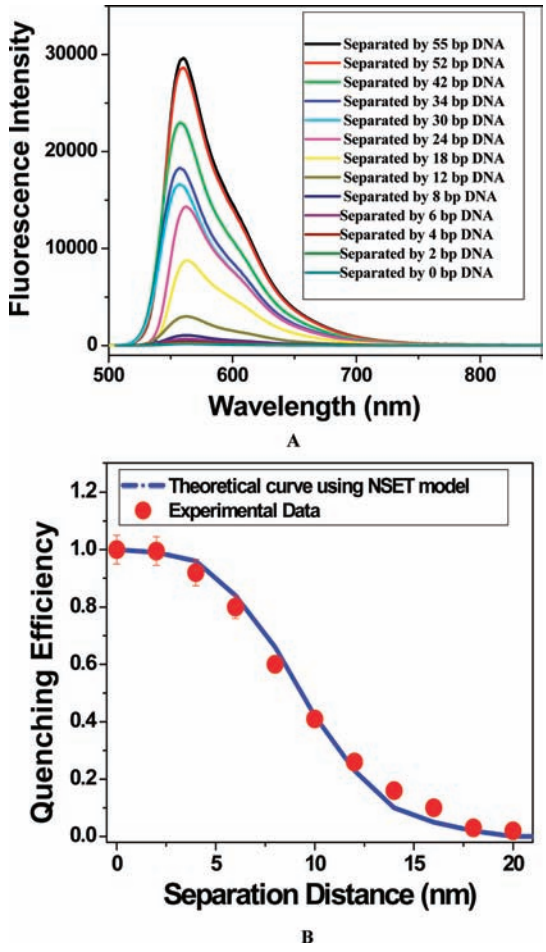

Figure 3. (A) Variation of fluorescence intensity for optical rulers of different lengths when Rh6G-modified dsDNAs of different lengths are attached to oval-shaped gold nanoparticles. (B) Variation of quenching efficiency with the distance between 30 nm oval-shaped AuNPs and Rh6G. Also shown are theoretical fitting data for the variation of the quenching efficiency with distance using the NSET formula in eq 3.

fluorescence peak due to the sample and control, and A_{smaple} and $A_{control}$ are the absorption values of the sample and control at the peak of the Rh6G dye. Our result clearly shows that a NSET ruler based on 30 nm oval-shaped AuNPs is highly sensitive to small changes in the Rh6G dye−particle distance even if they are separated by 20 nm, which is 2 times larger than the general FRET distance. To understand the distant-dependent quenching process for oval-shaped AuNPs, we tried to fit our data with the theoretical modeling using dipole-to-nanoparticle surface energy transfer as described by Jenning et al.[5] In case of NSET, the quantum efficiency of energy transfer can be written as[5−11]

$$\Phi_{ET} = \frac{1}{1 + (R/R_0)^n} \quad (3)$$

where R is the distance between donor and acceptor and R_0 is the distance between donor and acceptor at which the energy transfer efficiency is 50% and $n = 4$, in case of NSET. As shown in Figure 3, our result indicates that the long-distance quenching rate can be better described with a $1/R^4$ distance dependence using the NSET model. For the NSET model we used $R_0 = 7.8$ nm.

Since the NSET model can be used to measure the optical ruler distance, before each SERS measurement we measured the optical ruler distance using NSET, and we found that duplex DNA lengths measured by NSET and modeled by a rigid-rod approximation match very well. Figure 4A shows how

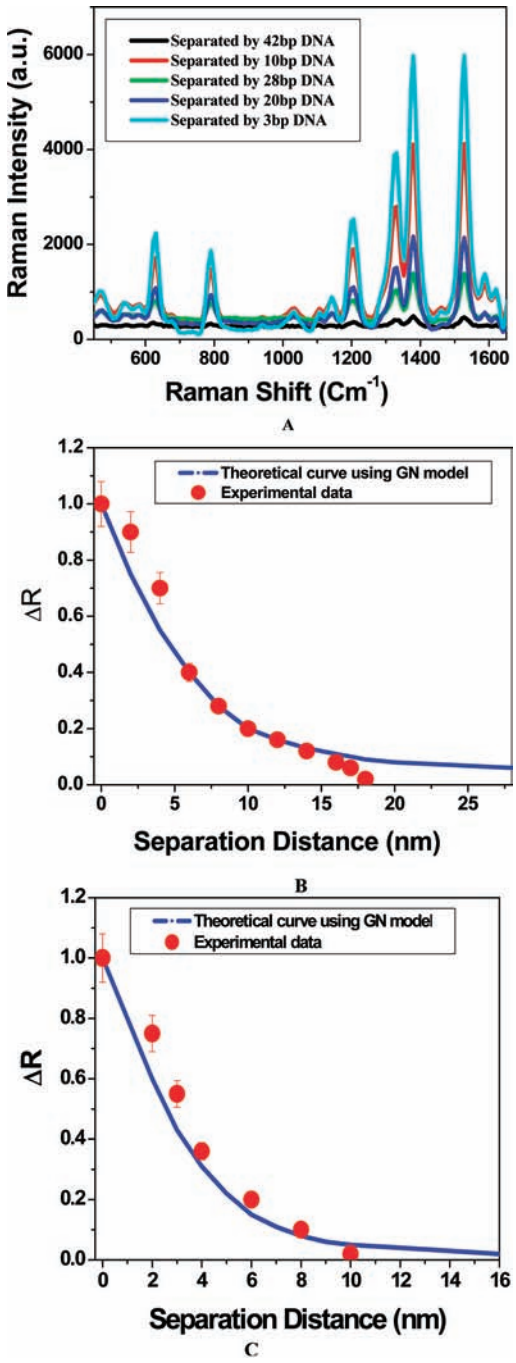

Figure 4. (A) Variation of the SERS intensity from Rh6G when the dye is separated from the oval-shaped gold nanoparticle surface using dsDNA of different lengths. (B) Variation of the SERS enhancement change (ΔR = SERS enhancement before and after separation) with the distance between 30 nm oval-shaped AuNPs and Rh6G dye when they are separated by dsDNA. (C) Variation of ΔR with the distance between 8 nm oval-shaped AuNPs and Rh6G dye when they are separated by dsDNA. Panels B and C also show theoretical fitting data for the variation of the Raman intensity with distance using the GN model.

SERS intensity changes as we move farther from the surface. Figure 4B shows how the change of SERS enhancement factor

dx.doi.org/10.1021/ja301921k | J. Am. Chem. Soc. 2012, 134, 8662−8669

(ΔR) varies with the distance, where ΔR is defined as the difference in the SERS enhancement before and after separation. Our result shows that the distance-dependent SERS is a quite long-range phenomenon. Though SERS has been known for almost 30 years, the SERS effect is still not fully understood.[18,28,29] Usually, the Raman signal enhancement in the presence of SERS-active substrate is attributed to two different effects.[21,27] First is the strong amplification of the electromagnetic fields near the plasmon resonances of metal substrates.[36−39] The electromagnetic enhancement effect usually depends on the evanescent nature of localized plasmon modes and can be significantly modified by surface imperfections.[28,29] The electromagnetic enhancement of Raman scattering E_{EM} can be expressed as[37−39]

$$E_{EM} \propto \left|\frac{E(\omega_0)}{E_0(\omega_0)}\right|^2 \left|\frac{E(\omega_{Raman})}{E_0(\omega_{Raman})}\right|^2 \quad (4)$$

where E_{EM} is the average enhancement over the surface, E and E_0 are the induced and incident electric fields from incident laser light, and ω_0 and ω_R are the incident laser frequency and Raman scattered frequency. According to eq 4, the electromagnetic enhancement factor is proportional to $\mathbf{E}(\omega)^4$. Second is the chemical enhancement effect, which is responsible for SERS. The chemical enhancement is mainly due to the electronic resonance process, where charge transfer occurs between the highest unoccupied molecular orbital of the molecules and the Fermi level of the metal substrate.[22,28,29] This charge-transfer enhancement is usually 12 orders of magnitude and is attributed to the surface−dye charge-transfer interaction.[41−43] As in our case the Raman dye is separated from the oval-shaped AuNPs surface by dsDNA, we can omit a chemical enhancement factor. Thus, here we describe only the electromagnetic enhancement contribution. Electromagnetic enhancement usually occurs when the local field oscillates at the frequency of the incident radiation used as a dipolar optical radiation source.[18,22,28,29] Also, the dipolar radiation scattered by the molecules near the surface is capable of coupling to the metal particle and enhancing the scattered light.[18,28,29] As a result, the distance-dependent SERS effect can be described as the dipolar field of the particle inducing a radiating dipole in the molecule, which is very similar to a London dispersion-type interaction.[18−21] Similarly, the distance dependence can be due to the dipole induced in the particle by the dipolar field of the scattering molecule. As a result, the overall distance dependence of the electromagnetic enhancement should be $1/r^{12}$, which indicates that the SERS should be a very short-range phenomenon.[18−21]

Our experimental results in Figure 4 show that SERS can be used as a long-range ruler. Our results clearly indicate that the SERS signal can be easily detectable when the Raman-active dyes are positioned at distances of more than 10 nm from the surfaces of the nanoparticles, which shows that the distance-dependent SERS cannot be explained using a $1/R^{12}$ distance dependence. Kennedy et al.[20] and Van Duyne et al.[18] reported that the distance-dependent electromagnetic enhancement of SERS for Ag using self-assembled monolayers of straight-chain alkanethiols can be explained using $1/R^{10}$ distance dependence, where R is the effective distance from the center of the surface to the Raman probe. Since a $1/R^{10}$ dependence cannot show any Raman signal after 4−5 nm, the long-distance SERS intensity change should be described with a longer-distance-dependent quenching than their $1/R^{10}$ characteristic for silver foil. As a result, we believe that for nanoparticles of large sizes, it is necessary to include near-field, induction, and radiation terms in the expression for a classical dipole radiator.

In general, the interactions between nanoparticles and Raman-active dye are quite complex due to the involvement of several parameters: excitation polarizations, wavelength, distance ranges, Raman-active dye characterization, nanoparticle surface coating, and particle shape and size.[4−11] Light induces oscillating dipole moments in each gold particle, and their instantaneous $(1/R)^3$ coupling results in a repulsive or attractive interaction, which obviously will modify the plasmon resonance of the system.[13−16] For that reason, the lesser dependence of the interaction strength on particle separation r results in a much longer interaction range compared to $1/R^{12}$ distance dependence, as we observed in our experiment. Next, to understand the experimental distance-dependent SERS phenomena, we also performed theoretical modeling using the GN model,[47] which is known to be useful when both the nanoparticle size (r) and the Raman dye-to-nanoparticle distance (d) are small compared to the excitation wavelength.[48−50] According to the GN model, the Raman cross section can be expressed as[48−51]

$$\sigma_{Raman} = \frac{8\pi}{3}\left(\frac{\omega}{c}\right)^4 (\Delta Q)^2 \left(\frac{\partial\alpha}{\partial Q}\right)^4 \left|\frac{1}{1-\alpha G}\left(1+\frac{2\alpha_i^{S}}{(r+d)}\right)\right|^4 \quad (5)$$

where σ_{Raman} is the Raman cross section at ω excitation frequency, α is the induced polarizability for the molecule due to the change of the nuclear coordinate (Q), and α_i is the ith-pole polarizability, which can be defined as[50,51]

$$\alpha_i = \frac{i(\varepsilon-\varepsilon_M)}{i\varepsilon+(i+1)}\alpha^{2i+1} \quad (6)$$

where α_i depends on metal dielectric constant ε, medium dielectric constant ε_M, and b^{2i+1}. In eq 5, G is the image-field factor, which can be defined as[48−51]

$$G = \sum_i \alpha_i^{S}\frac{(i+1)^2}{(r+d)^{2i+4}} \quad (7)$$

The SERS enhancement ratio, which we define as the ratio of σ_{Raman} in the presence and absence of nanoparticle, can be expressed as[48−51]

$$R = \left|\frac{1}{1-\alpha G}\left(1+\frac{2\alpha_1^{S}}{(r+d)^3}\right)\right|^4 \quad (8)$$

For the calculation of $\varepsilon(\omega)$, we used the Drude model with damping factor γ, due to electron scattering, as shown below:[48−51]

$$\varepsilon(\omega) = 1 - \frac{\omega_p^{2}}{\omega(\omega+i\gamma)} \quad (9)$$

where ω is the laser excitation frequency and ω_p is the plasmon frequency for nanoparticle.

Figure 4B,C shows how the SERS enhancement change (ΔR) varies with distance. It is very fascinating to note from Figure 4B,C that the trend of distance-dependent SERS enhancement change can be explained adequately using the simple GN model.

dx.doi.org/10.1021/ja301921k | J. Am. Chem. Soc. 2012, 134, 8662−8669

Next, to understand whether the distance-dependent SERS depends also on the size of the particle, we performed the same experiment with 8 nm AuNPs. Figure 4C shows how the SERS enhancement change varies with increasing distance between 8 nm oval-shaped AuNPs and Rh6G dye. Our result shows that the distance-dependent SERS is highly dependent on the particle size. The distance dependence of SERS intensity change for 8 nm oval-shaped AuNPs can be better described with the much faster distance-dependent Raman enhancement quenching. As we discussed before, according to the GN model, the Raman cross section should depend on the size of the particle. Therefore, we used the GN model to explain the size-dependent changes in the Raman ruler distance. The trend of the distance-dependent SERS enhancement change for 8 nm AuNPs also can be explained adequately using the simple GN model. So, our results indicate that one can tune the SERS ruler length between 8 and ∼20 nm by choosing the size of oval-shaped AuNPs. One has to remember that due to the effects of the surface charge, surface coverage, mutual strand interaction, and interaction with AuNPs, the apparent length of the DNA can be a little smaller than the expected molecular length. But since we calibrated the length with respect to NSET data, we believe that the above error will be insignificant, if any.

CONCLUSION

In this article, we report the development of a rigid SERS nanoruler using oval-shaped gold nanoparticles and Rh6G dye separated by dsDNA. Though SERS is often thought of as a near-field phenomenon, our reported data show that a SERS ruler based on oval-shaped AuNPs is highly sensitive to small changes in the dye−particle distance through dsDNA, even if they are separated by more than 15 nm. Our distance-dependent SERS intensity change data show that the distance dependence of the Raman intensity change is better described with a much longer distance-dependent quenching than the classical $1/R^{12}$ characteristic. Our theoretical modeling results indicate that the long-distance SERS intensity change for 30 nm oval-shaped AuNPs can be better described with the classical GN model. We also demonstrate that the distance-dependent SERS ruler length is highly dependent on the particle size. Our results show that one can tune the SERS ruler length between 8 and ∼20 nm by choosing the size of oval-shaped AuNPs. Since plasmonic nanomaterials are known to exhibit a great range of variability in their sizes and shapes, and systematic tunability of their optical plasmonic bands, the examples of the development of a SERS ruler in this article can be readily generalized to other plasmonic nanoparticles. The long-range SERS ruler developed by us can provide a spectral fingerprint of larger biological structures and will be useful for understanding structural dynamics like RNA and protein folding and DNA/RNA−protein interactions.

AUTHOR INFORMATION

Corresponding Author

paresh.c.ray@jsums.edu

Notes

The authors declare no competing financial interest.

ACKNOWLEDGMENTS

P.C.R. thanks NSF-PREM (grant no. DMR-0611539) and NSF-CREST (grant no. HRD-0833178) for their generous funding.

REFERENCES

(1) Stryer, L.; Haugland, R. P. *Proc. Natl. Acad. Sci. U.S.A.* **1967**, *58*, 719−725.
(2) Kaschak, D. M.; Mallouk, T. E. *J. Am. Chem. Soc.* **1996**, *118*, 4222−4223.
(3) Hagerman, P. J. *Annu. Rev. Biophys. Biophys. Chem.* **1988**, *17*, 265−286.
(4) Chen, Y.; O'Donoghue, M. B.; Huang, Y. F.; Kang, H.; Phillips, J. A.; Chen, X.; Estevez, M. C.; Yang, C. J.; Tan, W. *J. Am. Chem. Soc.* **2010**, *132*, 16559−16570.
(5) Jennings, T. L.; Singh, M. P.; Strouse, G. F. *J. Am. Chem. Soc.* **2006**, *128*, 5462−5467.
(6) Singh, M. P.; Strouse, G. F. *J. Am. Chem. Soc.* **2010**, *132*, 9383−9391.
(7) Seelig, J.; Leslie, K.; Renn, A.; Kuhn, S.; Jacobsen, V.; van de Corput, M.; Wyman, C.; Sandoghdar, V. *Nano Lett.* **2007**, *7*, 685−689.
(8) Chen, J. I. L.; Chen, Y.; Ginger, D. S. *J. Am. Chem. Soc.* **2010**, *132*, 9600−9601.
(9) Griffin, J.; Singh, A. K.; Senapati, D.; Rhodes, P.; Mitchell, K.; Robinson, B.; Yu, E.; Ray, P. C. *Chem.—Eur. J.* **2009**, *15*, 342−351.
(10) Griffin, J.; Ray, P. C. *J. Phys. Chem. B* **2008**, *112*, 11198−11201.
(11) Singh, A. K.; Lu, W.; Senapati, D.; Khan, S. A.; Fan, Z.; Senapati, T.; Demeritte, T.; Beqa, L.; Ray, P. C. *Small* **2011**, *7*, 2517−2525.
(12) Liu, G. L.; Yin, Y.; Kunchakarra, S.; Mukherjee, B.; Gerion, D.; Jett, D. S.; Bear, D. G.; Gray, J. W.; Alivisatos, P. A.; Lee, L. K. *Nature Nanotechnol.* **2006**, *1*, 47−52.
(13) Sönnichsen, C.; Reinhard, B. M.; Liphardt, J.; Alivisatos, A. P. *Nat. Biotechnol.* **2005**, *23*, 741−745.
(14) Jain, P. A.; Huang, W.; El-Sayed, M. A. *Nano Lett.* **2007**, *7*, 2080−2088.
(15) Rong, G.; Wang, H.; Reinhard, B. M. *Nano Lett.* **2010**, *10*, 230−238.
(16) Yun, C. S.; Javier, A.; Jennings, T.; Fisher, M.; Hira, S.; Peterson, S.; Hopkins, B.; Reich, N. O.; Strouse, G. F. *J. Am. Chem. Soc.* **2005**, *127*, 3115−3119.
(17) Dulkeith, E.; Ringler, M.; Klar, T. A.; Feldmann, J.; Muñoz, J. A.; Parak, W. J. *Nano Lett.* **2005**, *5*, 585−589.
(18) Dieringer, J. A.; McFarland, A. D.; Shah, N. C.; Stuart, D. A.; Whitney, A. V.; Yonzon, C. R.; Young, M. A.; Zhang, X.; Van Duyne, R. P. *Faraday Discuss.* **2005**, *132*, 9−26.
(19) Lal, S.; Grady, N. K.; Goodrich, G. P.; Halas, N. J. *Nano Lett.* **2006**, *6*, 2338−2343.
(20) Kennedy, B. J.; Spaeth, S.; Dickey, M.; Carron, K. T. *J. Phys. Chem. B* **1999**, *103*, 3640−3646.
(21) Bonham, A. J.; Braun, G.; Pavel, I.; Moskovits, M.; Reich, N. *J. Am. Chem. Soc.* **2007**, *129*, 14572−14573.
(22) Moskovits, M. *Rev. Mod. Phys.* **1985**, *57*, 783−826.
(23) Deng, X.; Braun, G. B.; Liu, S.; Sciortino, P. F.; Koefer, B.; Tombler, T.; Moskovits, M. *Nano Lett.* **2010**, *10*, 1780−1786.
(24) Xie, W.; Herrmann, C.; Kömpe, K.; Haase, M.; Schlücker, S. *J. Am. Chem. Soc.* **2011**, *133*, 19302−19305.
(25) Musumeci, A.; Gosztola, D.; Schiller, T.; Dimitrijevic, N. M.; Mujica, V.; Martin, D.; Rajh, T. *J. Am. Chem. Soc.* **2009**, *131*, 6040−6041.
(26) Goddard, G.; Brown, L. O.; Habbersett, R.; Brady, C. I.; Martin, J. C.; Graves, S. W.; Freyer, J. P.; Doorn, S. K. *J. Am. Chem. Soc.* **2010**, *132*, 6081−6090.
(27) Kleinman, S. L.; Ringe, E.; Valley, N.; Wustholz, K. L.; Phillips, E.; Scheidt, K. A.; Schatz, G. C.; Van Duyne, R. A. *J. Am. Chem. Soc.* **2011**, *133*, 4115−4122.
(28) Haran, G. *Acc. Chem. Res.* **2010**, *43*, 1135−1143.
(29) Brus, L. *Acc. Chem. Res.* **2008**, *41*, 1742−1749.
(30) Ray, P. C. *Chem. Rev.* **2010**, *110*, 5332−5365.
(31) Liu, X.; Dai, Q.; Austin, L.; Coutts, J.; Knowles, G.; Zou, J.; Chen, H.; Huo, Q. *J. Am. Chem. Soc.* **2008**, *130*, 2780−2782.
(32) Agasti, S. S.; Chompoosor, A.; Chang-Cheng, Y.; Ghosh, P.; Kim, C. K.; Rotello, V. M. *J. Am. Chem. Soc.* **2009**, *131*, 5728−5729.
(33) Sha, M. Y.; Xu, H.; Natan, M. J.; Cromer, R. *J. Am. Chem. Soc.* **2008**, *130*, 17214−17215.

(34) Wei, W.; Li, S.; Millstone, J. E.; Banholzer, M. J.; Chen, X.; Xu, X.; Schatz, G. C.; Mirkin, C. A. *Angew. Chem., Int. Ed.* **2009**, *48*, 4210−4212.
(35) Huang, Y.-F.; Liu, H.; Xiong, X.; Chen, Y.; Tan, W. *J. Am. Chem. Soc.* **2009**, *131*, 17328−17334.
(36) Qian, X.; Zhou, X.; Nie, S. *J. Am. Chem. Soc.* **2008**, *130*, 14934−14935.
(37) Brown, S. D.; Nativo, P.; Smith, J. A.; Stirling, D.; Edwards, P. R.; Venugopal, B.; Flint, D. J.; Plumb, J. A; Graham, D.; Wheate, N. J. *J. Am. Chem. Soc.* **2010**, *132*, 4678−4684.
(38) Camden, J. P.; Dieringer, J. A.; Zhao, J.; Van Duyne, R. P. *Acc. Chem. Res.* **2008**, *41*, 1653−1661.
(39) Dasary, S. S. R.; Singh, A. K.; Senapati, D.; Yu, K.; Ray, P. C. *J. Am. Chem. Soc.* **2009**, *131*, 13806−13812.
(40) Yu, H. J.; Javier, D.; Yaseen, M. A.; Nitin, N.; Richards, K. R.; Anvari, B.; Wong, M. S. *J. Am. Chem. Soc.* **2010**, *132*, 1929−1938.
(41) Morton, S. M.; Jensen, L. *J. Am. Chem. Soc.* **2009**, *131*, 4090−4098.
(42) Maitani, M. M.; Douglas, A. A.; Li, Z.; Allara, D. L.; Stewart, D. R.; Williams, S. R. *J. Am. Chem. Soc.* **2009**, *131*, 6310−6311.
(43) Park, W. H.; Kim, Z. H. *Nano Lett.* **2010**, *10*, 4040−4048.
(44) Berg, M. A.; Coleman, R. S.; Murphy, C. J. *Phys. Chem. Chem. Phys.* **2008**, *10*, 1229−1242.
(45) Clegg, R. M.; Murchie, A. I. H.; Zechel, A.; Lilley, D. M. J. *Proc. Natl. Acad. Sci. U.S.A.* **1993**, *90*, 2994−2998.
(46) Hagerman, P. J. *Annu. Rev. Biophys. Biol.* **1988**, *17*, 265−286.
(47) Gersten, J.; Nitzan, A. *J. Chem. Phys.* **1980**, *73*, 3023.
(48) Goude, E. Z.; Leung, P. T. *Solid State Commun.* **2007**, *143*, 416−420.
(49) Yin, Y. D.; Gao, L.; Qiu, C. W. *J. Phys. Chem. C* **2011**, *115*, 8893−8899.
(50) Rojas, R.; Claro, F.; Fuchs, R. *Phys. Rev. B* **1988**, *37*, 6799.
(51) Chang, R.; Leung, P. T. *Phys. Rev. B* **2006**, *73*, 125478.
(52) Grady, N. K.; Halas, N. J.; Nordlander, P. *Chem. Phys. Lett.* **2004**, *399*, 167.
(53) Wang, S.; Singh, A. K.; Senapati, D.; Neely, A.; Yu, H.; Ray, P. C. *Chem.—Eur. J.* **2010**, *16*, 5600−5606.
(54) Nikoobakht, B.; Wang, J.; El-Sayed, M. A. *Chem. Phys. Lett.* **2002**, *366*, 17−23.
(55) Orendorff, C. J.; Murphy, C. J. *J. Phys. Chem. B* **2006**, *110*, 3990−3994.
(56) Wijaya, A.; Schaffer, S. B.; Pallares, I. G.; Schifferli, K. H. *ACS Nano* **2009**, *3*, 80−86.
(57) Lu, W.; Singh, A. K.; Khan, S. A.; Senapati, D.; Yu, H.; Ray, P. C. *J. Am. Chem. Soc.* **2010**, *132*, 18103−18104.